45°K.[36] However, this interpretation now appears to be invalid not only because of the existence of the rise effect, but also because long-range interstitial motion in tungsten does not seem to occur until about 45°K. Finally, although the exact nature of the rise-effect mechanism is not clear, comparison of Figs. 6 and 8 indicates that the irradiation-induced background decrement anneals during close-pair recovery substages, suggesting that close-pair configurations are essential to the mechanism. The background reductions between 35 and 45°K might then be interpreted as the disappearance of defect-dislocation interactions through mutual annihilation of the close-pair constituents. On the other hand, the decrement increases near 26°K might suggest the conversion of one close-pair configuration into another more stable configuration which in its interaction with dislocations produces a larger decrement.

V. CONCLUSIONS

For an applied stress frequency of about 600 Hz, the results of the present research on Stage I in tungsten have revealed the existence of a prominent irradiation-induced internal-friction peak near 30°K. Peak properties such as its temperature half-width, dependence on stress direction, apparent independence of dislocation background, and radiation doping, and disappearance during close-pair resistivity recovery imply that it was produced by the stress-induced ordering of close-pair interstitials. Directional-dependence results suggest that the 30°K interstitials are not trigonal defects, that is, crowdions, but probably are orthorhombic defects in general and ⟨110⟩ split interstitials in particular. The split configuration for this interstitial is also supported by activation energy determinations which show its reorientation energy to be lower than its migration energy. In fact, were it not for a combination of this latter result and the low-observation temperature, internal-friction measurements in the employed frequency range would probably not have detected the interstitial at all. This conclusion is especially true in the case of electron irradiation since at these low irradiation temperatures it becomes impractical to use electrons to produce total defect concentrations greater than those attained here ($\sim 10^{-4}$). Nevertheless, the present results do suggest that, given a high enough defect concentration and a low enough stress frequency, self-interstitials in the bcc metals, like impurity interstitials, can be detected and studied by internal-friction techniques.

[36] J. A. DiCarlo, C. L. Snead, Jr., and A. N. Goland, Bull. Am. Phys. Soc. 13, 381 (1968).

ACKNOWLEDGMENTS

The authors wish to acknowledge the experimental assistance of the Dynamitron technicians and J. Palmer of the Instrumentation Department. One of the authors (J.A.D.) would like to express his thanks to the National Aeronautics and Space Administration for its financial support during the latter stages of this work.

PHYSICAL REVIEW VOLUME 178, NUMBER 3 15 FEBRUARY 1969

Singularities in the X-Ray Absorption and Emission of Metals. I. First-Order Parquet Calculation

B. ROULET, J. GAVORET, AND P. NOZIÈRES
Groupe de Physique des Solides E.N.S., Faculté des Sciences de Paris, 9, Quai Saint Bernard, Paris (5è), France*
(Received 22 August 1968)

X-ray emission and absorption spectra in metals may display singularities near the Fermi-level threshold. These singularities, predicted by Mahan, are due to final-state interactions between conduction electrons and the localized disturbance created by the x ray. The effect is treated within a simple model by the methods of perturbation theory. It is shown that even to lowest order one must sum the so-called parquet diagrams, in close analogy with the Abrikosov theory of the Kondo effect. Mahan's prediction is confirmed, and its validity discussed. Various secondary effects which could blur the singularity are analyzed.

I. INTRODUCTION

THE problem of x-ray absorption or emission in solids has been widely studied in the past thirty years. It has been recognized at an early stage that the electron interaction played an important role. For instance, in the ordinary Auger effect, the x-ray transition is accompanied by the excitation of one extra electron (giving rise to satellite lines and to spectral broadening). Sometimes the Auger effect may display a *collective resonance*, the excited electron being replaced by a plasmon.[1] A detailed review of these various phenomena has been given by Parratt.[2]

In metals, the emission and absorption spectra dis-

* Laboratoire Associé au Centre National de la Recherche Scientifique.

[1] P. Longe and A. J. Glick (to be published).

[2] L. G. Parratt, Rev. Mod. Phys. 31, 616 (1959).

play a sharp threshold corresponding to the edge of the Fermi distribution (possible broadening of this threshold will be discussed later). It has been suggested recently by Mahan[3] that the x-ray spectra should be singular near that threshold; let $(\omega-\omega_0)$ be the distance to threshold. By calculating the first terms of a perturbation expansion, and guessing what the sum should be, Mahan predicts that the absorption (emission) intensity should vary as $(\omega-\omega_0)^{-2g}$, where g is a dimensionless coupling constant, describing the interaction between conduction electrons and the deep hole left behind. Such a striking behavior is again a consequence of *final-state interactions* in the x-ray process. However, it arises from the discontinuity of the electron distribution at the Fermi level, and is, therefore, quite different from the usual Auger effect.

Such a singularity linked to the Fermi discontinuity is reminiscent of the Kondo effect. In the latter case, scattering of conduction electrons on a magnetic impurity is singular when the energy approaches the Fermi level. The singularity arises because the impurity has internal structure (i.e., its spin). Similarly, in the x-ray problem, the deep localized level is a *two-state system* (empty or full). The corresponding scattering amplitude of conduction electrons displays the same resonance as in the Kondo effect, which leads to Mahan's singularity. The resemblance between the two problems is particularly clear when the magnetic impurity is described in terms of Abrikosov's[4] "pseudo-fermion" operators. Such an analogy has been stressed by Anderson[5] and Hopfield[6] (who also established some general theorems on the overlap of many-body wave functions with different impurity potentials).

Our purpose is to apply to the x-ray problem the perturbation technique devised by Abrikosov[4] to deal with the Kondo effect. As in the latter problem, systematic search for singular factors leads one to solve coupled Bethe-Salpeter equations in *two* channels, the so-called "parquet" problem. In the simplest approximation, used by Abrikosov, one selects only the most divergent terms of the perturbation expansion; this part of the calculation is carried out in the present paper, and confirms the result guessed by Mahan. In a second article,[7] we shall show that such a procedure is not valid very close to the threshold. It is then necessary to carry out a self-consistent renormalization of all the singularities, which leads to somewhat different results (in agreement with those of Anderson[5]).

In fact, one does not need such a "many-body" approach in the x-ray case. Once the deep hole has been created, it acts as a *structureless* scattering center for conduction electrons (there is no "memory" of the hole between two collisions). One then has an essentially *one-body* problem, but a *transient* one: One wants to study the transient response to the sudden creation of a scattering center (while in the ordinary impurity problem one studies the adiabatic response to the scattering potential). Such a one-body approach is in fact much simpler; it may be carried through exactly, for arbitrary coupling strengths, and will be reported elsewhere.[8] However, it cannot be transposed to the Kondo effect, where the spin memory between two collisions is essential. For that reason, the many-body approach described in the present papers remains extremely useful, even though more complicated and far less elegant. It lays the ground, in a simple case, for *the self-consistent calculation of singular factors*, associated with resonant scattering near the Fermi level. A similar approach should be relevant in any problem involving logarithmic divergences. For instance, the sort of renormalization that we shall carry through is expected to be very important in the Kondo effect.

II. FORMULATION OF THE PROBLEM

We consider a metal, whose conduction electrons are assumed free, with creation operators $a_{\mathbf{k}}^\dagger$, energy $\epsilon_{\mathbf{k}}$. For simplicity, we ignore the electron spin, which can be restored at the end by inserting a few factors of 2. The Coulomb interaction *between conduction electrons* is neglected; since we are interested only in the vicinity of the Fermi level, it would only replace electrons by quasiparticles, with renormalized $a_{\mathbf{k}}^\dagger$ and $\epsilon_{\mathbf{k}}$. We assume that this renormalization has been carried through.

When an x-ray, with frequency ω, is absorbed, it excites one electron from a deep level to the conduction band. In the reverse emission process, a conduction electron fills the deep hole. We assume that the deep electron level is *localized* on a given lattice site: Thus there is no overlap of core wave functions from one site to the next, and the corresponding band of Bloch states is infinitely narrow (which corresponds to Mahan's assumption of an infinite hole mass). Let $b^\dagger$ and E_0 be the creation operator and energy of the deep electron level *before* the interaction with conduction electrons has been taken into account. The coupling with the x-ray field leads to a perturbing term in the Hamiltonian

$$H_X=\sum_{\mathbf{k}} W_{\mathbf{k}} a_{\mathbf{k}}^\dagger b e^{-i\omega t}+\text{c.c.} \tag{1}$$

When the deep level is empty, translational invariance is broken down, and the hole may scatter conduction electrons. Hence there appears a new term in the Hamiltonian

$$H_1=\sum_{\mathbf{k}\mathbf{k}'} V_{\mathbf{k}\mathbf{k}'} a_{\mathbf{k}}^\dagger a_{\mathbf{k}'} b b^\dagger, \tag{2}$$

which describes the rearrangement of conduction elec-

[3] G. D. Mahan, Phys. Rev. **163**, 612 (1967).
[4] A. A. Abrikosov, Physics **2**, 5 (1965).
[5] P. W. Anderson, Phys. Rev. Letters **18**, 1049 (1967).
[6] J. J. Hopfield (private communication).
[7] P. Nozières, J. Gavoret, and B. Roulet, following paper, Phys. Rev. **178**, 1084 (1969).
[8] P. Nozières and C. T. de Dominicis, second following paper, Phys. Rev. **178**, 1097 (1969).

trons in the potential of the hole. In the form (2), H_1 appears as a *many-body* interaction, added to the unperturbed part

$$H_0=\sum_{\mathbf{k}} \epsilon_{\mathbf{k}} a_{\mathbf{k}}^\dagger a_{\mathbf{k}}+E_0 b^\dagger b. \tag{3}$$

In its form (2), H_1 describes only the *intraband* part of the Coulomb interaction between all electrons. There exist, in fact, many other terms associated with band-to-band transitions, internal Auger effect, etc. We neglect them, as they do not contribute to the Mahan singularity studied here.

In order to calculate the x-ray transition rate, we introduce the response function

$$S(t-t')=\langle 0|T\{H_X(t)H_X(t')\}|0\rangle. \tag{4}$$

$H_X(t)$ is evaluated in the Heisenberg representation, using the total Hamiltonian (H_0+H_1). T denotes the usual time ordering operator. $|0\rangle$ is the "ground state" of the conduction electrons with the deep level either *filled* (for an absorption process) or *empty* (for an emission process). The transition rate is then proportional to the imaginary part of the Fourier transform $S(\omega)$.[9]

In order to calculate $S(\omega)$, we must make simplifying assumptions on the form of $V_{\mathbf{k}\mathbf{k}'}$. We shall take it as a separable potential of the BCS type:

$$V_{\mathbf{k}\mathbf{k}'}=-Vu_{\mathbf{k}}u_{\mathbf{k}'}, \quad \text{with} \quad \begin{aligned} u_{\mathbf{k}}&=1 \quad \text{if} \quad |\epsilon_{\mathbf{k}}-\mu|<\xi_0 \\ &=0 \quad \text{if} \quad |\epsilon_{\mathbf{k}}-\mu|>\xi_0. \end{aligned} \tag{5}$$

μ is the chemical potential, ξ_0 is a cutoff of order μ. With this definition, V is positive, corresponding to an electron hole attraction. (5) is a reasonable approximation to the *average* of $V_{\mathbf{k}\mathbf{k}'}$ over the angle between $\mathbf{k}$ and $\mathbf{k}'$, and should thus describe fairly well S-wave scattering by the deep hole. On the other hand, any scattering amplitude with $l\neq 0$ is obviously left out of (5). The strength of the interaction (2) is measured by the dimensionless parameter

$$g=\nu_0 V, \tag{6}$$

where ν_0 is the density of states at the Fermi level for a given spin. Taking for $V_{\mathbf{k}\mathbf{k}'}$ a screened Coulomb interaction, we find for g

$$g=\nu_0\left\langle \frac{4\pi e^2}{q_D^2+(\mathbf{k}-\mathbf{k}')^2}\right\rangle,$$

where q_D is the Debye wave vector. For a typical metal, g seems to lie between 0.1 and 0.5.

In the same spirit, we shall assume that $W_{\mathbf{k}}$ does not depend on $\mathbf{k}$.[10] Here, again, we miss all the information

[9] See, for instance, Ref. 3.

[10] In all but the zero-order term, the summation over k will be cut off by the interaction vertex (5). In the zero-order term itself, k is bound to be near the Fermi surface if ω is near the threshold. We may thus "cut off" W_k when $|\epsilon_k-\mu|>\xi_0$ without modifying the result. We shall use this corrected form which renders the calculation more symmetrical.

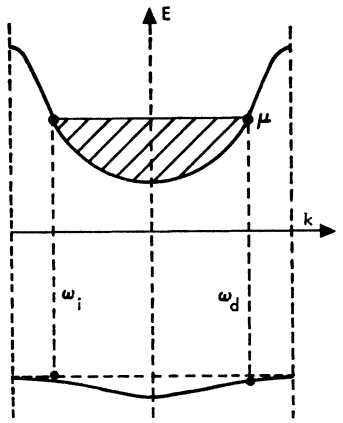

FIG. 1. The direct (ω_d) and indirect (ω_i) threshold frequencies when the deep state has a finite band width.

related to the angular symmetry of the core and conduction levels. All the subtle differences between K, L, M, $\cdots$ absorption lines are washed out, as well as considerations on the nature of conduction orbitals (s, p, d type ?). It does not appear difficult to extend our calculation by making a careful partial-wave analysis around the scattering center. However, for the sake of simplicity, we did not attempt it. In their present form, our results thus predict only the qualitative shape of the spectrum singularities.

It should be realized that besides the angular dependence of all factors, we are neglecting a number of other important physical effects. We already mentioned the neglect of "band broadening" of the deep level. Put another way, we assume the deep hole has no recoil. If we gave a small width Δ to the "energy band" of deep states, there would exist *two* threshold frequencies, as shown on Fig. 1. ω_d refers to direct transitions, where momentum is conserved, while ω_i refers to Auger transitions where an extra electron can pick up any momentum $<2k_F$ at no energy expense. Detailed analysis shows that Mahan's singularity is then spread over a distance Δ. The effect will usually be negligible, except for very shallow levels.

In the opposite limit of deep levels, one must worry about the lifetime of the deep hole. In emission, we implicitly assumed it was infinite, since we took the initial "ground state" $|0\rangle$ as well defined. In absorption, a finite lifetime τ will cut off the response function $S(t)$. In both cases, Mahan's singularity will be blurred over a range $1/\tau$. For very deep (e.g., K) levels, radiative recombination is dominant; corresponding lifetimes are very short ($<10^{-15}$ sec, see Ref. 2) and preclude the observation of Mahan's singularities, especially in heavy elements. For intermediate levels, radiative lifetimes may be reasonable, but then, one must worry about nonradiative recombination. The latter is due to internal Auger processes, and arises from interaction terms of the form

$$b^\dagger a^\dagger c_1 c_2,$$

where the two destruction operators c_1 and c_2 refer to conduction states, or more likely to other deep core states. Such terms were ignored in (2) because they involve large energy transfers; as was mentioned earlier, they do not contribute to the Mahan divergence, which involves very small energy transfers [terms of (2) with $\epsilon_k \approx \epsilon_{k'} \approx \mu$]. Still they can give rise to *real* transitions, and thus blur singularities.

The experimental situation is thus somewhat critical. The core state involved in the transition must not be too shallow (for fear of band broadening), nor too deep (because of lifetime broadening). Whether internal Auger effect is negligible in intermediate levels probably requires quantitative discussion in each case. It seems that Mahan's singularity exists in Al, Mg, and, to a lesser extent, in Na. A systematic analysis throughout the periodic table has not been attempted. Here we only wish to emphasize the limitations of our theory.

Let us now return to our simple "model" problem, where all the above difficulties are ignored. If there were no interaction H_1, the threshold frequency for both absorption and emission would be $(\mu - E_0)$; the transition rate would be proportional to the density of states (since we have assumed W_k constant). The inclusion of H_1 leads to *final-state interactions* which modify the spectrum. In absorption, the conduction electrons interact with the newly created hole. In emission, the static hole potential has been incorporated in $|0\rangle$, which involves scattering states rather than plane wave states. There remains a perturbation

$$-\sum_{kk'} V_{kk'} a_k^\dagger a_{k'} b^\dagger b, \tag{2'}$$

which describes how the scattering states adjust to the sudden destruction of the scattering center. According to Mahan, such final-state interactions lead to major *vertex corrections*, giving rise to an infinite transition probability at the threshold (Fig. 2). We shall indeed substantiate this result. However, we should not forget about possible self-energy corrections in the final state. Let us first consider *conduction* levels. Because the hole potential is localized, their energy is shifted by a quantity of order $1/N$, which is negligible. In principle, the hole potential might accept a bound state below the bottom of the conduction band, or a virtual bound state slightly above the bottom (where the broadening effect of the continuum is not too large). Actually, Mott[11] has pointed out that such bound states are not likely to exist, as they would require low electronic densities at which the system would no longer be metallic. Anyhow, they would occur far from the Fermi surface, in a region in which we are not interested.

In contrast, the deep level is localized; its energy is thus largely modified by the interaction (2), going from E_0 to a renormalized value E. Moreover, creating or destroying a deep electron breaks the equilibrium of

[11] N. F. Mott (to be published).

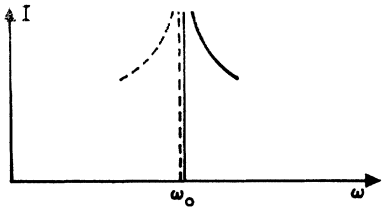

FIG. 2. The transition rate I near threshold ω_0, as a function of x-ray frequency ω. Dashed line: emission, full line: absorption.

conduction electrons, which may be excited in the process at a small energy expense. The deep level is thus *broadened asymmetrically*. A convenient way to characterize this broadening is to introduce the Green's function for the deep electron,

$$\mathcal{G}(t-t') = i\langle 0 | T\{b(t)b^\dagger(t')\} | 0\rangle. \tag{7}$$

$\mathcal{G}$ vanishes for $t>t'$ in an absorption experiment, for $t<t'$ in an emission experiment. The spectral density of the deep level is proportional to the imaginary part of the Fourier transform $\mathcal{G}(\epsilon)$. It extends from E to the low- or high-energy side, respectively, for the absorption or emission case. Such a broadening of the deep level tends to smooth the singularity near threshold; however, the latter remains sharp, since the spectral density of $\mathcal{G}$ is discontinuous at $\epsilon = E$. This "smearing" effect will be discussed in detail in the following paper.

The threshold in the x-ray spectrum occurs at $\omega_0 = \mu - E$. In the framework of perturbation theory, it is not obvious that ω_0 should be the same in absorption and emission. If, however, we interpret ω_0 as the difference in ground-state energies without and with the holes, the existence of a unique threshold becomes obvious: There is no "Stokes shift." This point is proven in Ref. 8.

III. PERTURBATION THEORY FORMALISM

Since the Mahan singularity occurs over an energy range $\gg kT$, we may restrict ourselves to the zero temperature limit. Together with the deep propagator $\mathcal{G}$, we introduce the conduction-electron Green's function

$$G_{kk'}(t-t') = i\langle 0 | T\{a_k(t)a_{k'}^\dagger(t')\} | 0\rangle. \tag{8}$$

In what follows, the renormalized $\mathcal{G}$ and $G_{kk'}$ will be denoted, respectively, by dashed and full lines. Because of the separable interaction (5), all the momentum variables are decoupled; only the following quantity will enter the calculation

$$G(t) = \sum_{kk'} u_k u_{k'} G_{kk'}(t). \tag{9}$$

The perturbation expansion is thus *one dimensional*, involving only energy variables. The basic interaction vertex is shown on Fig. 3(a). We wish to calculate the self-energies of $\mathcal{G}$ and G, sketched on Figs. 3(b) and 3(c),

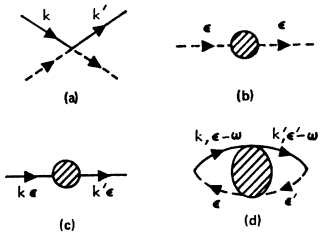

FIG. 3. (a) The basic interaction vertex, (b) a deep-electron self-energy, (c) a conduction-electron self-energy, (d) a contribution to the response function $\chi(\omega)$. Dashed and full lines refer, respectively, to deep- or conduction-electron propagators.

as well as the response function $S(\omega)$, given by all graphs of Fig. 3(d) (summed over ϵ, ϵ', $\mathbf{k}$, and $\mathbf{k}'$).

We note that only *one* deep electron (or hole) is involved. Thus the propagator $\mathcal{G}$ runs in only *one* time direction (forward in emission, backward in absorption). In any graph, there is only *one* open dashed line, and no deep-electron closed loop (except for first-order "Hartree" loops, shown on Fig. 4, which occur only in emission). We conclude that in absorption the propagator $G_{\mathbf{k}\mathbf{k}'}$ is unrenormalized, its Fourier transform being

$$G_{\mathbf{k}\mathbf{k}'}(\epsilon)=G_{\mathbf{k}0}\delta_{\mathbf{k}\mathbf{k}'}=\delta_{\mathbf{k}\mathbf{k}'}\frac{1}{\epsilon_{\mathbf{k}}-\epsilon-i\delta\,\mathrm{sgn}(\epsilon-\mu)}. \quad (10a)$$

In emission, G corresponds to propagation in the *static* deep-hole potential

$$G_{\mathbf{k}\mathbf{k}'}(\epsilon)=G_{\mathbf{k}0}(\epsilon)\delta_{\mathbf{k}\mathbf{k}'}+G_{\mathbf{k}0}(\epsilon)t_{\mathbf{k}\mathbf{k}'}(\epsilon)G_{\mathbf{k}'0}(\epsilon), \quad (10b)$$

$t_{\mathbf{k}\mathbf{k}'}(\epsilon)$ is the usual t matrix, easily calculated for the separable potential (5)

$$t_{\mathbf{k}\mathbf{k}'}(\epsilon)=Vu_{\mathbf{k}}u_{\mathbf{k}'}/[1-V\sum_{\mathbf{k}''}G_{\mathbf{k}''0}(\epsilon)u_{\mathbf{k}''}]. \quad (11)$$

Let us for simplicity assume that the density of conduction states is constant in the interaction range $(-\xi_0, +\xi_0)$ around the Fermi surface. In the absorption case, the quantity $G(\epsilon)$, defined in (9) is equal to

$$G(\epsilon)=\nu_0 f_0(\epsilon),$$

where

$$f_0(\epsilon)=\int_{\mu-\xi_0}^{\mu+\xi_0}\frac{d\epsilon_{\mathbf{k}}}{\epsilon_{\mathbf{k}}-\epsilon-i\delta\,\mathrm{sgn}(\epsilon-\mu)}$$

$$=\ln\left|\frac{\xi_0-(\epsilon-\mu)}{\xi_0+(\epsilon-\mu)}\right|+i\pi\theta(\epsilon-\mu), \quad (12a)$$

$$\theta(x)=\mathrm{sgn}x \quad \text{if} \quad |x|<\xi_0$$
$$=0 \quad \text{if} \quad |x|>\xi_0.$$

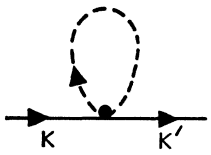

FIG. 4. The first-order conduction self-energy graph in the emission case.

(The singular behavior arises from the discontinuity of θ at $x=0$.) In the emission case, we find from (10b) and (11)

$$G(\epsilon)=\nu_0 f(\epsilon),$$
$$f=f_0/(1-gf_0). \quad (12b)$$

The discontinuity at $\epsilon=\mu$ remains.[12]

Since there is only one deep-electron line in the diagrams of Fig. 3(d), we may choose *independently* the origin of energy for the deep and conduction electrons. Let us measure the conduction-electron energy from μ (i.e., we set $\mu=0$). We, moreover, measure the deep-electron energy from the edge E of its spectral density: The branch point of $\mathcal{G}(\epsilon)$ then lies at $\epsilon=0$. With these conventions, the x-ray frequency ω, appearing in Fig. 3(d), is measured from $\omega_0=\mu-E$, that is, from the *threshold* of the x-ray spectrum. Hereafter, we shall only use these reduced variables; we shall retain the same notations, and thus make the replacements

$$\begin{aligned}&\epsilon_{\mathbf{k}}-\mu,\ \epsilon-\mu\longrightarrow\epsilon_{\mathbf{k}},\ \epsilon && \text{for conduction electrons}\\ &\epsilon-E\longrightarrow\epsilon && \text{for the deep electron}\\ &\omega-\omega_0\longrightarrow\omega && \text{for the x-ray frequency.}\end{aligned} \quad (13)$$

By doing so, we automatically ignore the *shift* of the threshold $E-E_0$ which is incorporated in the unspecified energy origins. Thus, we cannot calculate the *position* of the threshold; on the other hand, our reduced variables are perfectly all right to calculate the *shape* of the spectrum near threshold.

Let us get rid of the x-ray matrix elements by writing the response function $S(\omega)$ in the form

$$S(\omega)=|W|^2\chi(\omega).$$

The simplest approximation to $\chi(\omega)$ is obtained by summing the "ladder" graphs of Fig. 5(a). This calculation was performed by Mahan,[13] and yields the following result:

$$\chi_{\mathrm{Lad}}(\omega)=\frac{\nu_0\chi_0(\omega)}{1-g\chi_0(\omega)}, \quad (14)$$

where $\chi_0(\omega)$ is the zeroth-order contribution to χ

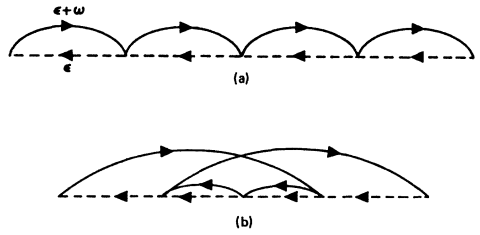

FIG. 5. (a) Ladder graphs in the calculation of $\chi(\omega)$, (b) extended ladder graphs allowing for propagation backward in time.

[12] Note that a bound state of conduction electrons would show up as a discrete pole of f, necessarily below the bottom of the conduction band, where $\mathrm{Im}f_0=0$.

[13] G. D. Mahan, Phys. Rev. 153, 882 (1967).

(within a factor ν_0)

$$\chi_0(\omega)=\int \frac{i}{2\pi}d\epsilon\, \mathcal{G}_0(\epsilon)f_0(\epsilon+\omega). \tag{15}$$

With our choice of energies, $\mathcal{G}_0=-1/\epsilon$. Because of the discontinuity of f_0, χ_0 is logarithmically divergent when $\omega\to 0$,

$$\chi_0\sim\frac{1}{2}\int\frac{d\epsilon}{\epsilon}\,\mathrm{sgn}(\epsilon+\omega)\sim\ln\frac{\xi_0}{\omega}. \tag{16}$$

In this "ladder" approximation, χ would vanish at threshold ($\omega=0$) and would display a discrete pole *below* threshold. This pole would correspond to a bound state of the conduction electron to the localized deep hole, lying at a distance $\xi_0\exp[-1/g]$ below the Fermi level. Such a bound state, lying in the continuum of filled conduction levels, is clearly unphysical (if it existed, it would be immediately broadened by excitation of other electrons). The error comes because the ladder graphs 5(a) only allow propagation of the excited conduction electron *forward in time*. Even with a static impurity potential, one would get such a bound state if one forced the electron to lie outside the *unperturbed* Fermi surface. Actually, this bound state disappears as soon as one allows propagation of the excited electron *backward* in time, as shown on Fig. 5(b). Physically, such graphs describe the excitation of several conduction electrons by the deep hole, which act to wash out the spurious pole of χ. Put another way, including only the ladder graphs 5(a) amounts to assuming a *rigid* Fermi sea (the exclusion principle acting on plane wave states). In a realistic calculation, the exclusion principle must, instead, be applied to the actual scattering states; the calculation must allow for the readjustment of all other electrons to the scattering potential, which is exactly what the graphs 5(b) achieve.[14]

That the graphs 5(a) and 5(b) are equally important is also obvious from a purely mathematical point of view. Let us consider the two basic "bubbles" of Figs. 6(a) and 6(b). We already found that the contribution of the bubble 6(a) was logarithmically divergent when $\omega=0$ [see (16)]. The contribution of bubble 6(b) has the form

$$\tilde{\chi}_0=\int\frac{i}{2\pi}d\epsilon\,\mathcal{G}_0(\epsilon)f_0(\omega-\epsilon)\sim-\ln\frac{\xi_0}{\omega}. \tag{17}$$

It is also divergent, with a sign opposite to that of χ_0. One might object that bubbles 6(b) with a *small* energy ω never enter in χ (since one integrates over all internal energies). However, a look at Fig. 6(c) shows that this is not true: For small ω, the integration over ϵ and ϵ' will provide two logarithmic factors; in building these

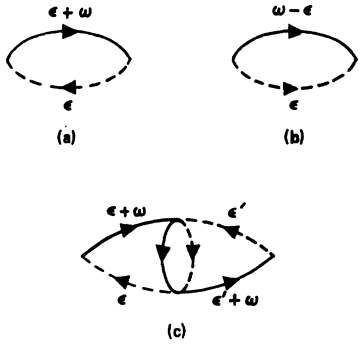

FIG. 6. (a) and (b): The two types of singular bubbles in the perturbation expansion, (c) a graph showing how singularities in the cross bubble are reflected in the response function $\chi(\omega)$.

logarithms, the important value of ϵ and ϵ' are of order ω; but then the total energy entering the cross bubble, $\epsilon+\epsilon'+\omega$, is also small, and a third logarithmic divergence appears. We thus conclude that the perturbation expansion of χ will contain an increasing number of logarithmically singular factors, arising from internal bubbles of *both* types 6(a) and 6(b). The inclusion of backward propagation [Fig. 5(b)] allows systematically for both types of singular bubbles, while the pure ladder graphs of Fig. 5(a) ignored all singularities associated with bubbles 6(b).

A decent calculation of the x-ray spectrum near threshold should trace systematically all logarithmic factors in the perturbation expansion, and then select the ones which are summed on a well-defined criterion. For instance, for weak coupling g, one may retain only the *most* divergent terms, proportional to $g^n\ln^{n+1}$. Such a program was achieved long ago by Diatlov, Sudakov, and Ter Martirosian,[15] in connection with the completely different problem of high-energy meson scattering. It proceeds in two steps.

(i) Write down *coupled* Bethe-Salpeter equations to describe multiple scattering of the deep and conduction electrons in the two singular "channels" (dashed and full lines parallel or antiparallel). All quantities are then expressed in terms of $\mathcal{G}$, G, and of an interaction kernel R which is irreducible in the *two* channels.

(ii) By taking the lowest-order terms of R, $\mathcal{G}$, and G, one sums the so-called "parquet" graphs, which incorporate the major logarithmic singularities of the expansion. The parquet graphs represent for the coupled channels what the ladder graphs are for a single scattering channel.

A similar approach has been applied by the Soviet-school to a number of problems (Kondo effect,[4] one-dimensional superconductivity[16]). It is required when-

[14] A similar situation is encountered in the theory of superconductivity. In his original paper, Cooper considers the motion of a bound pair outside a *rigid* Fermi sea, and finds a bound state below the Fermi level. Actually, one must allow for the propagation of the pair backward in time (i.e., for virtual excitation of other pairs from the Fermi sea): In the correct calculation, the spurious bound state is replaced by the usual pair instability.

[15] I. T. Diatlov, V. V. Sudakov, and K. A. Ter-Martirosian, Zh. Eksperim. i Teor. Fiz. **32**, 767 (1957) [English transl.: Soviet Phys.—JETP **5**, 631 (1957)].

[16] Yu. A. Bychkov, L. P. Gor'kov, and I. M. Dzyaloshinskii, Zh. Eksperim. i Teor. Fiz. **50**, 738 (1966) [English transl.: Soviet Phys.—JETP **23**, 489 (1966)].

ever singular factors occur in several different scattering channels.

In Sec. IV, we shall write down the general parquet equations, describing multiple scattering in the two "singular channels," without any approximation. In Sec. V, we solve these equations in the lowest approximation, valid for small coupling g and not too small energy ω ($g^2 \ln\xi_0/\omega \ll 1$); such an approximation is equivalent to that used in Refs. 4, 15, and 16. In the following paper, we present a more refined self-consistent calculation, which is claimed to work down to $\omega=0$.

IV. PARQUET ALGEBRA

Let γ be the renormalized interaction operator given by all graphs of Fig. 7. From γ one can calculate all quantities of interest. The total energy in channel 1 (parallel full and dashed lines) is equal to

$$\xi=\epsilon_1+\epsilon_1'=\epsilon_2+\epsilon_2'.$$

Similarly, the total energy in channel 2 (antiparallel full and dashed lines) is

$$\eta=\epsilon_1-\epsilon_2'=\epsilon_2-\epsilon_1'.$$

The energy variables of γ will be defined by specifying the two deep level energies ϵ_1 and ϵ_2, and the total energy ξ or η, in the channel of interest. Thus depending on the problem, we shall use either of the two following forms:

$$\gamma=\gamma(\epsilon_1,\epsilon_2,\xi)=\bar{\gamma}(\epsilon_1,\epsilon_2,\eta). \tag{18}$$

We note that the four variables are not independent, since $\epsilon_1+\epsilon_2=\xi+\eta$.

Let I_1 and I_2 be the sum of all graphs which are *irreducible* in respectively channels 1 and 2, while γ_1 and γ_2 are the sum of all graphs which are *reducible* in either channel. Clearly, we have

$$\gamma=I_1+\gamma_1=I_2+\gamma_2 \tag{19}$$

(since a graph is either irreducible or reducible). Here again, we shall use notations I_i, $\bar{I}_i$, γ_i, $\bar{\gamma}_i$, depending on the energy variables which are used [see (18)]. Typical graphs of γ_1 and γ_2 are shown on Figs. 8(a) and 8(b). We have singled out the first intermediate bubble starting from the incoming deep line: The left hand blocks are thus irreducible kernels I_1 and I_2, while on the right we have the full interaction operator γ. By looking at Fig. 8, we may write two usual Bethe-Salpeter equations for each channel separately

$$\gamma_1(\epsilon_1,\epsilon_2,\xi)=\frac{i}{2\pi}\int d\epsilon_i I_1(\epsilon_1,\epsilon_i,\xi)\mathcal{G}(\epsilon_i)G(\xi-\epsilon_i)\gamma(\epsilon_i,\epsilon_2,\xi),$$
$$\bar{\gamma}_2(\epsilon_1,\epsilon_2,\eta)=\frac{i}{2\pi}\int d\epsilon_i \bar{I}_2(\epsilon_1,\epsilon_i,\eta)\mathcal{G}(\epsilon_i)G(\epsilon_i-\eta)\bar{\gamma}(\epsilon_i,\epsilon_2,\eta). \tag{20}$$

We note that in (20) $\mathcal{G}$ and G are renormalized propagators.

We now remark that a given graph of γ cannot be

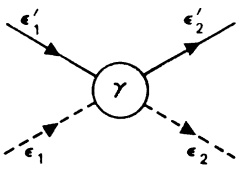

FIG. 7. The general renormalized interaction vertex.

reducible simultaneously in the two channels 1 and 2. [For instance, a graph of Fig. 8(a) should take the form of Fig. 9 if it were to be reducible in channel 2: This is clearly impossible because of particle conservation.] Thus, if we denote by R the sum of all graphs which are irreducible in both channels—the so-called totally irreducible interaction—we may write

$$\begin{aligned} I_1&=R+\gamma_2,\\ I_2&=R+\gamma_1,\\ \gamma&=R+\gamma_1+\gamma_2. \end{aligned} \tag{21}$$

To the extent that R, G, and $\mathcal{G}$ are known, (20) and (21) form a closed set of equations, from which one may, in principle, calculate all properties of interest. We note that these "parquet" equations are *exact*. They correspond to *coupled* Bethe-Salpeter equations in channels 1 and 2. Multiple scattering in the *two* channels is now built in, even if we use the simplest approximation for R. In contrast, an ordinary Bethe-Salpeter treatment in, say, channel 1 would express everything in terms of I_1, which remains singular because of multiple scattering in channel 2. The necessity of a *parquet reduction* is thus quite obvious.

The first term of R is the basic vertex of Fig. 3(a). As an illustration, the next two graphs of R are indicated on Fig. 10. (We note that the absence of closed dotted loops severely limits possible graphs.) In addition to R, one must know the self-energy Σ of the deep electron in order to calculate the propagator $\mathcal{G}$. We shall see in the following paper that it is essential to maintain consistent approximations in the calculation of Σ and R.

γ obeys a simple symmetry relation which is useful to check our results. Let us reverse the arrows of all conduction-electron lines and change their energies from ϵ_i' to $-\epsilon_i'$. Energy conservation at each vertex is thereby preserved. On the other hand, we have seen in (12a) that the zeroth-order propagator G was an *odd* function of energy. Since a graph of γ of order n contains $(n-1)$ conduction-electron lines, it follows that

$$\gamma(\epsilon_1,\epsilon_2,\epsilon_1',\epsilon_2';g)=-\gamma(\epsilon_1,\epsilon_2,-\epsilon_2',-\epsilon_1';-g). \tag{22}$$

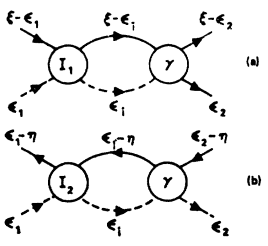

FIG. 8. Reducible graphs contributing respectively to γ_1 (a) and γ_2 (b). The first intermediate bubble from the left has been singled out.

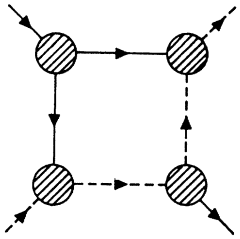

FIG. 9. An *impossible* graph which would be reducible in both channels 1 and 2.

Similarly, a glance at Fig. 8 shows that

$$\gamma_1(\epsilon_1,\epsilon_2,\xi;\, g)=-\bar{\gamma}_2(\epsilon_1,\epsilon_2,\xi;\, -g). \tag{23}$$

These relations are exact, but depend on our particular choice of $V_{kk'}$ (symmetric with respect to the Fermi level).

V. FIRST-ORDER SOLUTION TO PARQUET EQUATIONS (WEAK COUPLING)

We assume that the coupling constant g is $\ll 1$. The first-order contribution to the interaction operator γ is $\gamma^{(1)}\sim V$. The second-order terms, given by graphs of Fig. 6(b), are of order

$$\gamma^{(2)}\sim VgL,$$
$$L=\ln(\xi_0/\epsilon),$$

where ϵ is the (small) total energy in either channel. (Were it not for the large factor L, $\gamma^{(2)}$ would be negligible.) More generally, an arbitrary term of the perturbation expansion will give a contribution of the form

$$Vg^nL^{n-p} \quad (p\geq 0).$$

The first approximation consists in selecting the *most divergent* terms of the expansion, that is those which correspond to $p=0$. Such an approximation will be valid as long as $gL\lesssim 1$: Then one must retain all terms of the form $V(gL)^n$, while a term such as Vg^2L is negligible. Put another way, the perturbation expansion of γ may be rearranged in the following way:

$$\gamma=V[\alpha_0(gL)+g\alpha_1(gL)+g^2\alpha_2(gL)+\cdots]. \tag{24}$$

In the first-order solution, one retains only the first term α_0 (g is a small parameter, while gL is not). Clearly, such an approximation is no longer valid when $L\gg 1/g$: For very large L, a term such as g^2L may, for instance, become larger than 1. Thus, the first-order solution to the parquet equations presented here is only valid for *not too small* energies, $\epsilon>\xi_0\exp[-1/g]$. When $\epsilon\to 0$, a more refined self-consistent treatment is required:

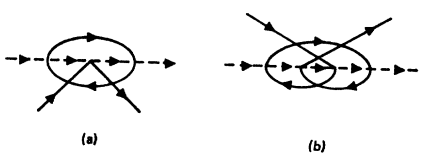

(a) (b)

FIG. 10. The third- and fourth-order contributions to the totally irreducible interaction R.

FIG. 11. The lowest graph of the deep level self-energy Σ.

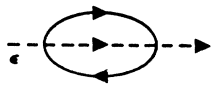

Such a calculation is described in the following paper.

We first consider the totally irreducible interaction R. The contribution of the two graphs of Fig. 10 may be calculated explicitly (see Ref. 7 for a detailed discussion); one finds that

$$R\sim Vg^2\ln(\xi_0/\epsilon) \quad [\text{Fig. 10(a)}]$$
$$\sim Vg^3\ln(\xi_0/\epsilon) \quad [\text{Fig. 10(b)}],$$

where ϵ is the *maximum* energy of the two deep lines entering or leaving γ. In our first-order approximation, such corrections are negligible as compared to the first term $R^{(1)}=V$. Such a conclusion persists to all orders (in an irreducible graph, the internal lines are so tightly linked together tha one cannot pile up enough *independent* logarithmic factors). The leading logarithmic terms will thus be obtained by setting

$$R=V. \tag{25a}$$

We now turn to the conduction-electron Green's function G. In (12b), the denominator of f introduces an extra factor g without any additional ln. To be consistent, we must neglect this term. Moreover, the logarithmic divergence arises *only* from the discontinuous imaginary part of f_0 (the real part vanishes when $\epsilon=\mu$). We shall thus write

$$G=\nu_0 i\pi\theta(\epsilon). \tag{25b}$$

Finally, the deep-electron Green's function is

$$\mathcal{G}=-1/(\epsilon+\tilde{\Sigma}),$$

where $\tilde{\Sigma}$ is the self-energy measured from its value at the branch point E

$$\tilde{\Sigma}(\epsilon)=\Sigma(\epsilon)-\Sigma(0)$$

[$\Sigma(0)$ gives rise to the shift $(E-E_0)$, and disappeared when we chose the origin $\epsilon=0$ at the *actual* branch point of $\mathcal{G}$]. The lowest graph of $\tilde{\Sigma}$ is shown on Fig. 11, its contribution is found to be of order

$$g^2\epsilon\ln(\xi_0/\epsilon).$$

Within our approximation it is negligible as compared to ϵ. The same conclusion holds to all orders: We shall thus write

$$\mathcal{G}=-1/(\epsilon\pm i\delta) \tag{25c}$$

(the sign $\pm$ corresponds, respectively, to x-ray emission or absorption). In practice, the δ-function part of (25c) does not contribute to the logarithmic divergence and may be discarded: We thus arrive at exactly the same equations in the absorption and emission cases.

The latter approximation is somewhat tricky, as imaginary parts are essential in order to define the analytic properties of the various quantities near branch cuts. When neglecting them, we can only obtain

the real (*reactive*) part of all operators. In the imaginary (*dissipative*) parts, one ln is replaced by $\pm i\pi$: The corresponding calculation would require a higher accuracy. Actually we know from general arguments how branch cuts should be disposed. We can then bypass the above difficulties by using relations of the Kramers-Kronig type between real and imaginary parts.

Within the above approximation, we sum all the so called "*parquet graphs*," which can be obtained from the first-order vertex by replacing any number of times a single vertex by a bubble of Fig. 6(a) *or* 6(b). A typical example of such a graph is shown on Fig. 12, together with its mechanism of formation. Every time a vertex is replaced by a bubble, the graph contribution is multiplied by a factor $\sim gL$. All parquet graphs will thus contribute terms of order

$$V(gL)^n,$$

in agreement with our approximation criterion.

Making use of these various approximations, the exact Eqs. (20) become

$$\gamma_1(\epsilon_1,\epsilon_2,\xi)=\frac{\nu_0}{2}\int\frac{d\epsilon_i}{\epsilon_i}\theta(\xi-\epsilon_i)I_1(\epsilon_1,\epsilon_i,\xi)\gamma(\epsilon_i,\epsilon_2,\xi)\,,$$
$$\bar\gamma_2(\epsilon_1,\epsilon_2,\eta)=\frac{\nu_0}{2}\int\frac{d\epsilon_i}{\epsilon_i}\theta(\epsilon_i-\eta)\bar I_2(\epsilon_1,\epsilon_i,\eta)\bar\gamma(\epsilon_i,\epsilon_2,\eta)\,; \tag{26}$$

$$I_1(\epsilon_1,\epsilon_i,\xi)=V+\bar\gamma_2(\epsilon_1,\,\epsilon_i,\,\epsilon_1+\epsilon_i-\xi)\,,$$
$$\bar I_2(\epsilon_1,\epsilon_i,\eta)=V+\gamma_1(\epsilon_1,\,\epsilon_i,\,\epsilon_1+\epsilon_i-\eta)\,. \tag{27}$$

The existence of logarithmic factors is quite clear; γ_1, for instance, contains an integral of the form

$$\int_\xi^{\xi_0}\frac{d\epsilon_i}{\epsilon_i}=\ln\frac{\xi_0}{\xi}. \tag{28}$$

Similarly, $\bar\gamma_2$ contains factors ln ξ_0/η. In addition, both γ_1 and $\bar\gamma_2$ depend on ϵ_1 and ϵ_2 through the irreducible kernels I. [Let us, for instance, consider the diagram of Fig. 12: ϵ_1 enters via the total energy in the cross bubble, which yields a factor $\sim\ln(\epsilon_1+\epsilon_i-\xi)$]. Each term γ_1 or γ_2 has its "natural independent variables," which ensure a reasonably smooth variation of the function; for γ_1, these are ϵ_1, ϵ_2, ξ, while for γ_2 they are ϵ_1, ϵ_2, η: That is why we chose to write (26) and (27) exclusively in terms of γ_1 and $\bar\gamma_2$.

We note that all energies enter through slowly varying logarithms. To the extent that we collect the *maximum* number of logarithms, two quantities like—

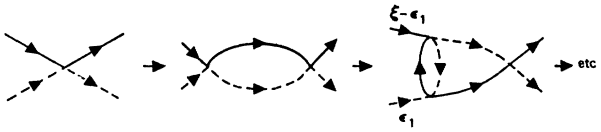

FIG. 12. An example of construction of successive parquet graphs.

say, lnξ and ln2ξ—are identical. Thus we need only define energies with *logarithmic accuracy* (i.e., within a factor of order 1). Let us, for instance, consider the factor $\ln(\epsilon_1+\epsilon_i-\xi)$ which appears in Fig. 12: Within the above accuracy, we may replace it by $\ln[\max(\epsilon_1-\xi,\,\epsilon_i)]$; such a replacement is wrong when $\epsilon_1-\xi\approx-\epsilon_i$, but such a range of ϵ_i gives a negligible contribution to the integral (28), which serves to build the factor lnξ. Moreover, the relevant values of ϵ_i in that integral are $>\xi$, so that we may perform the replacement (again within logarithmic accuracy)

$$\ln(\epsilon_1+\epsilon_i-\xi)\to\ln[\max(\epsilon_1,\epsilon_i)].$$

Such a *logarithmic approximation* will be carried out everywhere; whenever we have quantity $\gamma(\epsilon_i+a)$, where ϵ_i is an integration variable, we replace it by $\gamma(\max(\epsilon_i,a))$. The corresponding error involves one less logarithm in the expansion, and is thus negligible in our first-order calculation.

With the above approximation, only the absolute values of ϵ_1, ϵ_2, ϵ_i, etc., enter the calculation. We can thus simplify the integrals according to

$$\int\frac{d\epsilon_i}{\epsilon_i}\theta(\xi-\epsilon_i)=-2\int_\xi^{\xi_0}\frac{d\epsilon_i}{\epsilon_i} \tag{29}$$

(remember that we are interested in the range $\xi\ll\xi_0$). Moreover, let us consider again the graph of Fig. 12: It clearly does not depend on ϵ_1 if $\epsilon_1\lesssim\xi$ [since in that case $\max(\epsilon_1,\epsilon_i)=\epsilon_i$]. Such a conclusion may be extended to all orders by induction—and anyhow it may be checked on the final result. A similar result holds for ϵ_2 (the two ends of the graph play symmetrical roles). We conclude that

$$\begin{aligned}\gamma_1(\epsilon_1,\epsilon_2,\xi)=\gamma_1(\xi,\epsilon_2,\xi)=\gamma_1(\epsilon_2,\xi)\quad&\text{if}\quad\epsilon_1<\xi<\epsilon_2\\ =\gamma_1(\xi,\xi,\xi)=\gamma_1(\xi)\quad&\text{if}\quad\epsilon_1,\,\epsilon_2<\xi\end{aligned} \tag{30}$$

(note the shorthand notation to avoid repetition of the same variable). A similar relation may be established for $\bar\gamma_2(\epsilon_1,\epsilon_2,\eta)$. By combining (30) with our general logarithmic approximation, we may transform (27) into

$$I_1(\epsilon_1,\epsilon_i,\xi)=V+\bar\gamma_2(\max(\epsilon_1,\epsilon_i))\,,$$
$$\bar I_2(\epsilon_1,\epsilon_i,\eta)=V+\gamma_1(\max(\epsilon_1,\epsilon_i))\,. \tag{31}$$

The passage from (27) to (31) is the key approximation of this paper. It is only valid to leading order in the logarithmic expansion, and will have to be reconsidered in the more sophisticated treatment of the following paper.

At this stage, it is convenient to replace ϵ_i by a new "logarithmic variable"

$$t_i=\ln(\xi_0/\epsilon_i). \tag{32}$$

In the same way, ϵ_1, ϵ_2, ξ, η are replaced by quantities t_1, t_2, α, β. We remember that $\epsilon_1+\epsilon_2=\xi+\eta$; thus t_1, t_2,

α, β are not independent, but instead obey the relation

$$\min(t_1,t_2)=\min(\alpha,\beta). \tag{33}$$

On using (29), we may write the basic equations (26) and (31) in the following (final) form:

$$\begin{aligned}\gamma_1(t_1,t_2,\alpha)&=-\nu_0\int_0^\alpha dt_i I_1[\min(t_1,t_i)]\\&\quad\times\{I_1[\min(t_2,t_i)]+\gamma_1(t_i,t_2,\alpha)\},\\ \bar\gamma_2(t_1,t_2,\beta)&=+\nu_0\int_0^\beta dt_i \bar I_2[\min(t_1,t_i)]\\&\quad\times\{\bar I_2[\min(t_2,t_i)]+\bar\gamma_2(t_i,t_2,\beta)\},\\ I_1(t)&=V+\bar\gamma_2(t),\quad \bar I_2(t)=V+\gamma_1(t).\end{aligned} \tag{34}$$

It is clear on (32) that γ_1 does not depend on t_1 when $t_1>\alpha$ (i.e., $\epsilon_1<\xi$): We thus confirm our earlier prediction (30).

The approximate equations (34) may be solved *exactly*, using a trick by Abrikosov[4] and Sudakov.[17] The solution is sketched in the Appendix, and yields the following result:

$$\begin{aligned}&\frac{1}{V}\gamma_1(t_1,t_2,\alpha)\\&=\tfrac{1}{2}\left[e^{-g|\min(\alpha,t_1)-\min(\alpha,t_2)|}+e^{-g[2\alpha-\min(\alpha,t_1)-\min(\alpha,t_2)]}\right]\\&\qquad-1-g\min(\alpha,t_1,t_2),\\&\frac{1}{V}\bar\gamma_2(t_1,t_2,\beta)\\&=\tfrac{1}{2}\left[e^{+g|\min(\beta,t_1)-\min(\beta,t_2)|}+e^{+g[2\beta-\min(\beta,t_1)-\min(\beta,t_2)]}\right]\\&\qquad-1+g\min(\beta,t_1,t_2).\end{aligned} \tag{35}$$

We note that (35) obeys the general symmetry relation (23); γ_1 tends to be exponentially small while $\bar\gamma_2$ is exponentially large (the opposite result would hold if we reversed the sign of the interaction). From γ_1 and γ_2, the total interaction γ is obtained by

$$\gamma=\gamma_1+\gamma_2+V.$$

The general result (35) is rather unappealing: We shall illustrate it on specific examples. Let us assume $t_1\leqslant t_2$ (this is not a real limitation, since γ_1 and γ_2 are obviously symmetrical in t_1 and t_2). From (33), it follows that

$$t_1=\min(\alpha,\beta).$$

Two cases are then possible

(i) $t_2\geqslant\max(\alpha,\beta)$: (35) simplifies considerably, and yields

$$\gamma=Ve^{g(\beta-\alpha)}, \tag{36}$$

(ii) $t_2<\max(\alpha,\beta)$: γ remains complicated, and the general form (35) must be explicited in each given case (as done for example in the following section).

Here we shall only discuss the particular result (36). We first note that $\gamma=V$ when $\alpha=\beta$; thus for comparable energies in the two channels, the singularities cancel out completely, and γ reduces to its first-order term. Such a cancellation was already apparent in second order, when we found that the two singular bubbles (16) and (17) had opposite signs. We, here, prove that the cancellation persists to all orders. This cancellation is very helpful, as it will simplify considerably the improved calculation of the following paper. Physically, it follows from the fact that the scattering potential, once created by the x-ray, is *structureless*. [In the Kondo effect for instance, the scattering potential has an internal degree of freedom (its spin), and the above cancellation no longer occurs, as shown by Abrikosov[4].]

When $\alpha\neq\beta$, the higher-order terms no longer cancel. The result (36) must be viewed as the sum of a perturbation expansion

$$1+g(\beta-\alpha)+\cdots=e^{g(\beta-\alpha)}.$$

The second term corresponds to the elementary bubbles (16) and (17). When expressed in terms of the original energy variables, (36) becomes

$$\gamma=V(\xi/\eta)^g.$$

γ is seen to have an essential singularity near the origin, with a rather unexpected exponent.

VI. RESPONSE FUNCTION AND X-RAY TRANSITION RATE

Knowing the interaction operator γ, it is straightforward to calculate the response function $\chi(\omega)$, given by all graphs of Fig. 3(d). On including the zeroth-order term, we may write

$$\begin{aligned}\chi(\omega)=\nu_0\int\left(-\frac{i}{2\pi}\right)d\epsilon\,\mathcal{G}(\epsilon)G(\epsilon-\omega)+\nu_0^2\int\left(\frac{i}{2\pi}\right)^2 d\epsilon\,d\epsilon'\\\times\mathcal{G}(\epsilon)G(\epsilon-\omega)\bar\gamma(\epsilon,\epsilon',\omega)\mathcal{G}(\epsilon')G(\epsilon'-\omega).\end{aligned} \tag{37}$$

Here again, we must treat the integrations over ϵ and ϵ' within logarithmic accuracy. Using the same approximations as in Sec. V, we transform (37) into

$$\chi(\omega)=\nu_0\beta+\nu_0^2\int_0^\beta dt\,dt'\bar\gamma(t,t',\beta), \tag{38}$$

where β is defined as

$$\beta=\ln\xi_0/\omega.$$

$\bar\gamma$ is symmetric under interchange of t and t', so that (38) may be replaced by

$$\chi(\omega)=\nu_0\beta+2\nu_0^2\int_0^\beta dt'\int_0^{t'}dt\,\bar\gamma(t,t',\beta). \tag{39}$$

[17] V. V. Sudakov, Dokl. Akad. Nauk SSSR **111**, 338 (1956) [English transl.: Soviet Phys.—Doklady **1**, 662 (1956)].

TABLE I. Determination of imaginary part of $\ln\xi_0/\omega$.

	$\omega>0$	$\omega<0$
Absorption	$i\pi$	0
Emission	0	$i\pi$

We now use the general result (35), noting that here $\alpha=t$, because of relation (33). On using (A4) and (A5), we obtain

$$\bar{\gamma}(t,t',\beta)=\gamma_1+\gamma_2+V=\tfrac{1}{2}V[e^{g(t'-t)}+e^{g(2\beta-t-t')}]. \quad (40)$$

We insert (40) into (39), and perform the integration which yields

$$\chi(\omega)=(\nu_0/2g)[e^{2g\beta}-1]. \quad (41)$$

Expressed in terms of the frequency ω itself, (41) becomes

$$\chi(\omega)=(\nu_0/2g)[(\xi_0/\omega)^{2g}-1]. \quad (42)$$

(42) is exactly the result guessed by Mahan[3] by extrapolating the first few terms of the expansion. We note the strong singularity of χ when $\omega\to 0$, which involves a power law with an exponent proportional to the interaction strength.

The x-ray transition rate is proportional to $\mathrm{Im}\chi$. To calculate it, we note that the branch cut of χ lies on the positive semiaxis for absorption (*above* the threshold), on the negative semiaxis for emission (*below* the threshold). This fixes the determination of $\ln(\xi_0/\omega)$, whose imaginary part is indicated in Table I.

The simplest way to calculate $\mathrm{Im}\chi$ is to add the relevant imaginary part to β in (41) [a correction which does not modify the main part of $\chi(\omega)$ within our logarithmic approximation]. We thus obtain

$$\mathrm{Im}\chi=\sin(2\pi g)(\nu_0/2g)e^{2g\beta}\eta(\pm\omega), \quad (43)$$

where η is the usual step function, and the sign $\pm$ corresponds respectively to absorption or emission. Actually, our calculation only makes sense when $g\ll 1$, so that we must rather write

$$\mathrm{Im}\chi(\omega)=\pi\nu_0 e^{2g\beta}\eta(\pm\omega)=\pi\nu_0(\xi_0/\omega)^{2g}\eta(\pm\omega). \quad (44)$$

The result (44) provides the shape of the x-ray spectrum near the threshold.

Another way to obtain $\mathrm{Im}\chi$, which may be less questionable than the above procedure, is to choose it in such a way that, when inserted in the Kramers-Kronig relation

$$\mathrm{Re}\chi(\omega)=-\frac{1}{\pi}\int\frac{\mathrm{Im}\chi(\omega')}{\omega-\omega'}d\omega', \quad (45)$$

it gives the right result (41). In the limit $g\ll 1$, to which we are restricted, such a fancy method gives the same answer (44).

VII. CONCLUSION

We have confirmed the prediction of Mahan[3] that there should exist a singularity of the x-ray absorption or emission spectrum near the Fermi level threshold. This singularity follows a power law, with an exponent proportional to the interaction strength. There is some experimental evidence of such an anomaly. However, before attempting a comparison with experiment, one must remember that we have neglected a number of corrections which would broaden such a "resonance" of the spectrum: lifetime of the deep-level band broadening (that is, diffusion of the hole to other lattice sites). The importance of such effects must be evaluated in each of the many specific cases.

A similar singularity (and the associated parquet graphs) should occur whenever a degenerate Fermi gas interacts with a discrete level (here with a localized state). Its physical origin lies in the very long time required by the electrons near the Fermi surface to readjust to a new localized environment. During that long time, these electrons keep exchanging with the electron initially excited by the x-ray, which tends to enhance the low-frequency part of the spectrum (that is, the part near threshold).

Throughout the paper, we have ignored the spin of conduction electrons. In the present approximation, where all graphs involve only one open electron line which bounces again and again on the deep hole, it only acts to double the density of states. Since the x-ray transition conserves spin, we only need to multiply the response function χ by a factor 2.

In principle, our calculation is only valid when $g\ln(\xi_0/\omega)\sim 1$, i.e., when the resonant enhancement of χ is not large. However, we shall see in the following paper that the theory can be extended down to $\omega=0$ by including self-energy and vertex renormalization in consistent fashion. Such a self-consistent treatment deeply modifies the nature of the singularities, which are no longer logarithmic at very low energies. Nevertheless, it does not affect markedly the shape of the x-ray spectrum, which remains very close to (44). Such an unexpected result comes from a nearly complete cancellation of self-energy and vertex corrections, and may be traced back to the tendency of the singularities in the two channels to cancel each other.

This large amount of cancelling singularities becomes very clear in the "one-body" treatment of the problem described in Ref. 8. There we obtain an exact solution for arbitrary coupling strength. One recovers a result of the type (44), g being simply replaced by δ/π, where δ is the s-phase shift at the Fermi surface.[18] Our main reason for developing at length the present "many-body" approach is that it serves as a pattern for more complicated problems, like the Kondo effect. In that respect, the renormalized calculation presented in the following paper should prove very useful.

[18] This feature guarantees that $\mathrm{Im}\chi$ is always positive, in contrast to (43) which, if extended to large g, would become negative.

ACKNOWLEDGMENTS

The authors wish to thank Professor A. A. Abrikosov and I. M. Dzialoshinski for a helpful discussion on the general structure of parquet expansions.

APPENDIX

According to (34), γ_1 is an iteration of any number $\geqslant 2$ of kernels I_1, separated by "bubbles," as shown on Fig. 13. Each bubble is characterized by a variable t_i $(0<t_i<\alpha)$. In a given graph, let us select the bubble with *the highest* t_i, which we take equal to t. On the right *and* left of that "maximum" bubble, there may exist any number of other bubbles $(\geqslant 0)$ with the restriction that their t_j be *all* smaller than t. On the right and left of the central bubble, we thus find a *full* γ; the restriction on t_j means that in these factors γ we must replace α by t. We may thus write the equation

$$\gamma_1(t_1,t_2,\alpha)=-\nu_0\int_0^\alpha dt[I_1(\min(t_1,t))+\gamma_1(t_1,t,t)]\times[I_1(\min(t_2,t))+\gamma_1(t,t_2,t)]. \quad \text{(A1)}$$

(A1) is completely equivalent to the first equation (34). We note that there is *no* duplication of diagrams: The procedure whereby we select the highest t_i is perfectly well defined, and effectively leaves a full γ on either side. The objection raised by Silverstein and Duke[19] is thus not valid. A similar equation holds for $\bar{\gamma}_2$

$$\bar{\gamma}_2(t_1,t_2,\beta)=\nu_0\int_0^\beta dt[\bar{I}_2(\min(t_1,t))+\bar{\gamma}_2(t_1,t,t)]\times[\bar{I}_2(\min(t_2,t))+\bar{\gamma}_2(t,t_2,t)]. \quad \text{(A2)}$$

Let us now consider the case $t_1, t_2\geqslant\alpha, \beta$: γ_1 and $\bar{\gamma}_2$ do not depend on t_1 and t_2 [which is indeed obvious on (A1) and (A2)]. On using the last equation (34), we may cast the above equations into the following simpler form:

$$\gamma_1(\alpha)=-\nu_0\int_0^\alpha dt[V+\bar{\gamma}_2(t)+\gamma_1(t)]^2,$$
$$\bar{\gamma}_2(\beta)=+\nu_0\int_0^\beta dt[V+\gamma_1(t)+\bar{\gamma}_2(t)]^2. \quad \text{(A3)}$$

From (A3), it follows at once that

$$\gamma(\alpha)=\gamma_1(\alpha)+\bar{\gamma}_2(\alpha)+V=V. \quad \text{(A4)}$$

As discussed in the text, the singular terms γ_1 and γ_2 completely *cancel* for comparable energies in the two channels. Using (A3) and (A4), one verifies that

$$\bar{\gamma}_2(\alpha)=-\gamma_1(\alpha)=Vg\alpha. \quad \text{(A5)}$$

Here again, all the terms with more than one logarithm have cancelled out.

We now consider a somewhat more complicated case

$$t_1<\alpha\leqslant t_2.$$

From (33), it follows that $\beta=t_1$, so that $\bar{\gamma}_2(t_1,t_2,\beta)=Vgt_1$. In (A1), we must distinguish the ranges $(0,t_1)$ and (t_1,α). On using (A4), together with the shorthand notation (30), we thus obtain

$$\gamma(t_1,\alpha)=V(1+gt_1)-\nu_0\left\{\int_0^{t_1}V^2dt+\int_{t_1}^\alpha V\gamma(t_1,t)dt\right\}. \quad \text{(A6)}$$

On differentiating with respect to t_1, (A6) gives rise to a simple differential equation

$$\partial\gamma/\partial t_1=+g\gamma.$$

Using the boundary condition $\gamma(t_1,\alpha)=V$ for $t_1=\alpha$, we find

$$\gamma(t_1,\alpha)=Ve^{g(t_1-\alpha)} \quad \text{(A7)}$$

in agreement with the result (36). A similar calculation yields the same result when $t_1<\beta\leqslant t_2$.

Let us finally assume $t_1<t_2<\alpha$. Again, (33) implies $\beta=t_1$ and $\bar{\gamma}_2=Vgt_1$. In (A1), we must now distinguish three regions, $(0,t_1)$, (t_1,t_2), and (t_2,α). Since the γ which enter the integral (A1) always have two energies equal, there may be obtained from (A7). We thus find

$$\gamma(t_1,t_2,\alpha)=V(1+gt_1)-\nu_0\left\{\int_0^{t_1}V^2dt+\int_{t_1}^{t_2}V^2e^{g(t_1-t)}dt+\int_{t_2}^\alpha V^2e^{g(t_1-t)}e^{g(t_2-t)}dt\right\}.$$

Integration is immediate and yields

$$\gamma(t_1,t_2,\alpha)=\tfrac{1}{2}V\{e^{g(t_1-t_2)}+e^{g(t_1+t_2-2\alpha)}\}. \quad \text{(A8)}$$

By looking at all possible orderings of variables, one finds the general result (35).

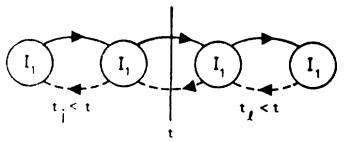

FIG. 13. The iteration of kernels I_1 contributing to γ_1. The vertical bar marks the bubble with the highest $t_i=t$. On either side there is any number of bubbles, all with $t_j<t$.

[19] S. D. Silverstein and C. B. Duke, Phys. Rev. **161**, 456 (1967).